AFRL-RZ-WP-TR-2008-2018

POWER AND THERMAL TECHNOLOGIES FOR AIR AND SPACE

Delivery Order 0003: Development of High-Performance Solid Oxide Fuel Cell (SOFC) Technology for Remote Base Applications

Haiming Xiao and Thomas Reitz

UES, Inc.

AUGUST 2007
Final Report

AIR FORCE RESEARCH LABORATORY
PROPULSION DIRECTORATE
WRIGHT-PATTERSON AIR FORCE BASE, OH 45433-7251
AIR FORCE MATERIEL COMMAND
UNITED STATES AIR FORCE

NOTICE AND SIGNATURE PAGE

Using Government drawings, specifications, or other data included in this document for any purpose other than Government procurement does not in any way obligate the U.S. Government. The fact that the Government formulated or supplied the drawings, specifications, or other data does not license the holder or any other person or corporation; or convey any rights or permission to manufacture, use, or sell any patented invention that may relate to them.

This report was cleared for public release by the Air Force Research Laboratory Wright Site (AFRL/WS) Public Affairs Office (PAO) and is available to the general public, including foreign nationals. Copies may be obtained from the Defense Technical Information Center (DTIC) (http://www.dtic.mil).

AFRL-RZ-WP-TR-2008-2018 HAS BEEN REVIEWED AND IS APPROVED FOR PUBLICATION IN ACCORDANCE WITH ASSIGNED DISTRIBUTION STATEMENT.

*//Signature//

THOMAS L. REITZ, Ph.D.
Chemical Engineer
Electrochemistry & Thermal Sciences

//Signature//

THOMAS L. REITZ, Ph.D.
Chief
Electrochemistry & Thermal Sciences

//Signature//

KIRK L. YERKES, Ph.D.
Deputy for Science
Power Division

This report is published in the interest of scientific and technical information exchange, and its publication does not constitute the Government's approval or disapproval of its ideas or findings.

*Disseminated copies will show "//Signature//" stamped or typed above the signature blocks.

REPORT DOCUMENTATION PAGE

Form Approved
OMB No. 0704-0188

1. REPORT DATE *(DD-MM-YY)*	2. REPORT TYPE	3. DATES COVERED *(From - To)*
August 2007	Final	01 March 2005 – 15 May 2007

4. TITLE AND SUBTITLE
POWER AND THERMAL TECHNOLOGIES FOR AIR AND SPACE
Delivery Order 0003: Development of High-Performance Solid Oxide Fuel Cell (SOFC) Technology for Remote Base Applications

5a. CONTRACT NUMBER
FA8650-04-D-2404-0003

5b. GRANT NUMBER

5c. PROGRAM ELEMENT NUMBER
62203F

6. AUTHOR(S)
Haiming Xiao (UES, Inc.)
Thomas Reitz (AFRL/RZPS)

5d. PROJECT NUMBER
3145

5e. TASK NUMBER
22

5f. WORK UNIT NUMBER
3145229Z

7. PERFORMING ORGANIZATION NAME(S) AND ADDRESS(ES)

UES, Inc.
4401 Dayton-Xenia Road
Dayton, OH 45432-1894

Electrochemistry and Thermal Sciences Branch (AFRL/RZPS)
Power Division
Air Force Research Laboratory, Propulsion Directorate
Wright-Patterson Air Force Base, OH 45433-7251
Air Force Materiel Command, United States Air Force

8. PERFORMING ORGANIZATION REPORT NUMBER

9. SPONSORING/MONITORING AGENCY NAME(S) AND ADDRESS(ES)
Air Force Research Laboratory
Propulsion Directorate
Wright-Patterson Air Force Base, OH 45433-7251
Air Force Materiel Command
United States Air Force

10. SPONSORING/MONITORING AGENCY ACRONYM(S)
AFRL/RZPS

11. SPONSORING/MONITORING AGENCY REPORT NUMBER(S)
AFRL-RZ-WP-TR-2008-2018

12. DISTRIBUTION/AVAILABILITY STATEMENT
Approved for public release; distribution unlimited.

13. SUPPLEMENTARY NOTES
Report contains color. PAO Case Number: WS 07-0044, 01 Mar 2007.

14. ABSTRACT
The longevity performance of a tape cast SOFC using a LSM-based cathode was studied for 500 hours at various power densities. Polarization experiments indicated an enhancement in performance during the long-term polarization. Electrochemical Impedance Spectroscopy (EIS) experiments were used to deconvolute the component impedances in the cell. The EIS data indicated that the vast majority of cell activation was associated with a single semi-circular feature which occurred in the low frequency region. Additional experiments were performed to attempt to assign specific electrode processes to corresponding semicircular features in the EIS spectra. These data suggest that steady polarization of the cell results in a gradual increase in cell performance which can be attributed to a ripening of the LSM-based cathode.

15. SUBJECT TERMS
fuel cells, Solid oxide fuel cells

16. SECURITY CLASSIFICATION OF:			17. LIMITATION OF ABSTRACT:	18. NUMBER OF PAGES	19a. NAME OF RESPONSIBLE PERSON (Monitor)
a. REPORT	b. ABSTRACT	c. THIS PAGE			Thomas L. Reitz
Unclassified	Unclassified	Unclassified	SAR	22	19b. TELEPHONE NUMBER *(Include Area Code)* N/A

Standard Form 298 (Rev. 8-98)
Prescribed by ANSI Std. Z39-18

Table of Contents

List of Figures iv
List of Tables iv
Executive Summary 1
Introduction 2
Experimental Details 3
Results 5
Discussion 12
Conclusion 13
References 14

List of Figures

Figure 1. Lifetime study of sample button cell 5
Figure 2. SEM Images of SOFC button cells at time 0 hr (a) and time 450 hr (b).....6
Figure 3. Voltage – Current Density Characteristics 7
Figure 4. Impedance spectroscopy of a SOFC cell during activation as measured at different times during operation at 750°C. 8
Figure 5. Example impedance spectrum with notional semicircular features illustrating the data analysis of a SOFC cell during activation (750°C). 9
Figure 6. Real component of impedance as a function of time-on-stream (750°C). 10
Figure 7. Impedance spectra of SOFC containing both a cathode interlayer and without cathode interlayer, Both specimens were measured at 800°C. 11

List of Tables

Table 1. Estimated Tafel parameters as a function of cell run-time 8

Executive Summary

The longevity performance of a tape cast solid oxide fuel cell using a LSM-based cathode was studied for 500 hours at various power densities. Polarization experiments indicated an enhancement in performance during the long term polarization. Electrochemical Impedance Spectroscopy (EIS) experiments were used to deconvolute the component impedances in the cell. The EIS data indicated that the vast majority of cell activation was associated with a single semi-circular feature which occurred in the low frequency region. Additional experiments were performed to attempt to assign specific electrode processes to corresponding semicircular features in the EIS spectra. These data suggest that steady polarization of the cell results in a gradual increase in cell performance which can be attributed to a ripening of the LSM-based cathode.

Introduction

Solid oxide fuel cells (SOFC) represent one of the most promising options for significantly increasing our energy conversion efficiencies in various applications including stationary power generation, household combined heat and power, and as automotive auxiliary power units (APUs) (i, ii). As such they are an area of intense research. Traditional SOFC required thick electrolytes to support the anode and cathode electrode and therefore required very high operating temperatures to provide sufficient ion conductivity for operation (iii). In recent years, however, anode supported electrode conformations with thin film electrolytes have been heavily explored because they are capable of far greater power densities (iv,v). These thin electrolyte approaches have necessitated the development of thin film interlayers wherein the cell composition is modified to promote an improved interaction between the bulk electrode and the thin film electrolyte (vi). It has been observed that the nature of these interlayers is complex and can exhibit substantial changes in performance during the lifetime of the cell (vii). One particular example relates to activation of cell whereby a SOFC cell containing a LSM-based cathode will exhibit an improvement in performance as the cell is polarized. This process has been known for some time but is only recently been studied to attempt to determine the precise nature of this ripening (viii). Several recent studies have examined this process in depth and the current understanding of cell activation is attributed to complex morphological modification of the cathode/electrolyte interface during polarization (ix,x). However, additional questions remain regarding this phenomenon. The objective of this study was to explore long term cell ripening process through investigation of polarization and electrochemical impedance spectroscopy. These data were used to clarify the role of the cathode/electrolyte interface on cell activation.

Experimental Details

Test cells were constructed through a five layer process which includes: (a) porous Ni+YSZ anode support; (b) anode/electrolyte interlayer; (c) dense YSZ electrolyte; (d) cathode/electrolyte interlayer; (e) porous LSM ($(La_{0.85}Sr_{0.15})_{0.98}$ Mn_{03-x}) cathode (x = 0.103). This study's focus was to evaluate the longevity of these cells while under galvanostatic control and to evaluate the changes in cell performance during this long term study. The interlayer compositions employed in this study were 50%YSZ-50%LSM for cathode/electrolyte and 50%YSZ-50%NiO for anode/electrolyte.

The cell fabrication process is briefed as follows: NiO and YSZ materials were purchased from Alfa Aesar and Tosoh respectively, and were mixed in non-aqueous slurry in requisite proportions (70% NiO -30% YSZ for anode and 50% NiO -50% YSZ for anode/electrolyte interlayer), and then ball milled with measured amounts of rice flour or carbon to induces porosity. The ball mill was conducted in a wet process with 5 mm diameter YSZ balls and ethanol-based solvent as media. After ball-mill, the slurries were separated from the ball media and dried for use as the materials for tape-cast. The tape-cast slurries of the anode, anode/electrolyte interlayer, and electrolyte were prepared via the following procedure. The dried powders were added to a solvated fish oil dispersant (Tape Casting Warehouse) and milled for 24 hours. Polyalkylene glycol (Tape Casting Warehouse) and polyvinyl butyral (Tape Casting Warehouse) were added to the milling solution and a second 24 hour mill process was performed. The slurries are then filtered and tape-cast to green tapes of desired thicknesses. The green anode, anode/electrolyte, and electrolyte tapes were isostatically laminated. A laser-cutter (Universal Laser Systems, Inc) was used to cut the laminated tape to discs of 3.2 cm in diameter. The three-layer discs were sintered in air at 1400 ºC for two hours, after which the discs had reduced in size to 2.5 cm in diameter. Cathode interlayer and LSM cathode slurries were then pasted onto the sintered three-layer sintered discs to complete the button cells. The cathode surface area was controlled to a known value so that the current density can be calculated for electrochemical measurements.

Four probe electrochemical measurements were achieved by attaching two platinum wires to each side of the button cell, i.e., anode and cathode. The anode supported button cell was sealed onto an alumina tube (Vesuvius) with high temperature cement (Cerambond 552, Aremco Products Inc.). A specially-designed quartz fixture for feeding fuel gas and releasing exhaust gas was connected to the alumina tube through a compression fitting (Swagelok). Sealing around the anode leads was accomplished through two threaded bushings with silicon rubber septums (ACE Glass) which were attached to the quartz fixture via a graded seal. The complete cell was then placed into the isothermal zone of a clam-shell furnace. Reduction of the NiO to Ni was achieved through a controlled temperature ramp in an anode flow stream of 10% H_2, balance N_2. Thermal Gravimetric Analysis (TGA) determined that 98% of NiO was reduced by 380 ºC in pure hydrogen suggesting that complete reduction of the anode would be achieved by 450 C. After the anode reduction was complete, the cell was brought to the desired temperature for testing and the reactant gas was switched to humidified hydrogen gas. The cathode chamber is not sealed, so purified air was blown over the surface to ensure

ample oxygen availability. Electrochemical characterization was conducted using Solartron 1260 Impedance gain/phase analyzer coupled to a Solartron 1287 Electrochemical Interface. Complete cell assemblies were evaluated electrochemically to ensure that hermeticity was achieved. Open circuit voltages (OCVs) were nominally 1.05 to 1.12V. A pictorial representation of the completed cell, the test fixture, and a more detailed description of cell continuity analysis are provided elsewhere (xi).

Results

The longevity of a SOFC button cell prepared via tape casting was explored at several different galvanostatic test regimes and the data are displayed as Figure 1. In an effort to simulate typical cell operating conditions, three scenarios were examined which include low, average, and high cell power densities (100, 300, and 600 mA/cm^2, respectively). Because the longevity runs were performed at constant current, voltage was allowed to fluctuate and was regarded as an indicator of cell performance. The temperature of the cell through the longevity study was maintained at 750°C. At designated intervals, the galvanostatic longevity experiment was interrupted to perform polarization and EIS experiments needed to provide additional information on cell health and performance. These interruptions were removed from Figure 1 to enhance clarity.

Upon inspection of Figure 1, it can be observed that initial cell potential was 849 mV at 100 mA/cm^2 but increased to 920 mV within the first 10 hours of operation. While the majority of the enhancement was observed during this initial period, some additional improvement continued during the entire galvanostatic longevity experiment. Initial power densities of 84.9 mW/cm^2 was observed at a current density of 100 mA/cm^2 but increased to 93.3 mW/cm^2 over the first 150 hours of test. After the cell was

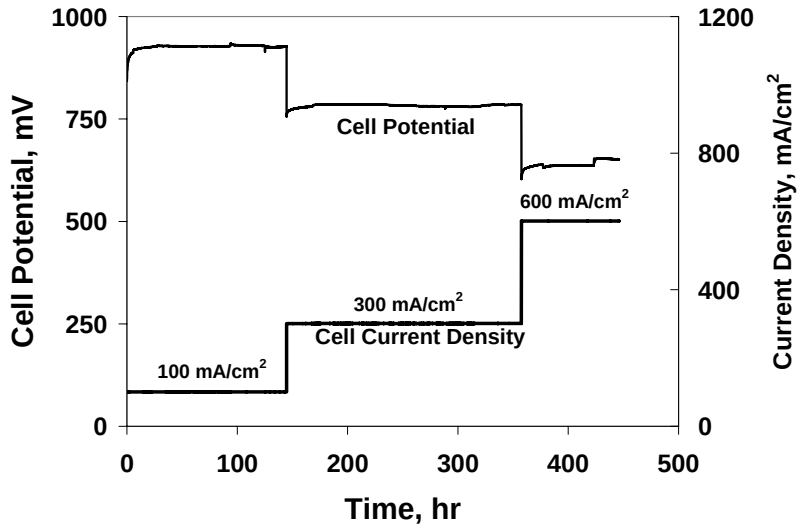

Figure 1. Lifetime study of sample button cell

characterized, the cell current was increased to 300 mA/cm^2 wherein a power density of 227.2 mW/cm^2 was observed. The cell was then allowed to operate galvanostatically for another 200 hours with average power densities exceeding 236 mW/cm^2. The cell was again characterized for performance after which the cell current density was increased to 600 mA/cm^2 and a cell power density of 363 mW/cm^2 was observed. Again, the cell was allowed to operate galvanostatically for another 100 hours until the test was concluded. Peak power densities under a constant 600 mA/cm^2 load were 393 mW/cm^2 at a cell polarization of 652 mV.

Scanning Electron Microscopy images taken at time 0 and after the 450 hour polarization experiment for prototypical button cell is presented as Figure 2 (a and b). Because the cell could not be imaged prior to polarization, a nearly identical cell was prepared, reduced and briefly operated to provide a baseline microscopy image. As can be observed from the micrographs, the electrolytes and interlayer thicknesses of the samples appear to be largely equivalent and provide a reasonable comparison between the two specimens. Electrolyte thicknesses for the pre-activated and post-treatment samples were 10 μm and 8 μm, respectively. Anode and cathode interlayers were approximately 20 μm for both specimens. The microscopy images clearly reflect a difference in particle size between bulk cathode and cathode interlayer which reflects a change in the porosity of the two layers.

High resolution microscopy images were not obtained and detailed a microscopy analysis was not performed on these specimens. However, within the limits of these images, no significant change was observed in the particle size or morphology which could be attributed to cathode activation during the longevity study. Previous authors, using high resolution SEM, have observed changes in interlayer morphology during the activation process (viii). A more detailed microscopy study to further clarify relationship between interlayer morphology and cell performance will be a subject of a future study.

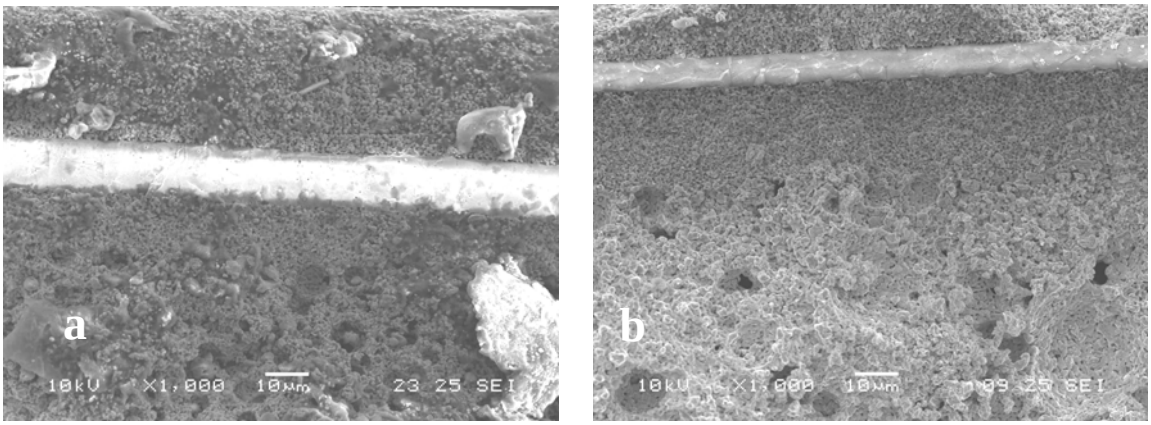

Figure 2. SEM Images of SOFC button cells at time 0 hr (a) and time 450 hr (b)

As discussed previously, the longevity run was periodically interrupted to observe the health of the cell through polarization and electrochemical impedance spectroscopy (EIS). Figure 3 shows the polarization curves for the button cells characterized at different run times. As is readily observed, the performance of the cells exhibits an increase in performance during operation. The majority of the polarization experiments were performed during the low current density run (100 mA/cm^2) which ran for 150 hours prior to switching to the intermediate cell current density (300 mA/cm^2). The performance of the cell gradually increased during this time wherein max power density went from 370 mW/cm^2 at 340 mV at the initial evaluation to 910 mW/cm^2 at 470 mV for the fully conditioned cell (250 hr). Cell polarization experiments continued through the 300 mA/cm^2 (350 hr) current density examination, however, only minor increases in

cell performance were observed and these data were omitted for clarity. Furthermore, it should be noted that some portion of the cell activation observed during polarization was lost when cell polarization was removed for long times (> 30 min). This indicates that cell activation is partially reversible and is likely associated with the generation of some electroactive entity such as an oxide ion vacancy which facilitates enhanced cell activity. What is noticeable from closer inspection of the polarization curves contained in Figure 3 is that the shape of the curve clearly changed as performance improved. This change in the curve shape, especially noticeable at higher current densities, may be indicative of the introduction of mass transfer effects specifically as the cell begins to reach power densities in excess of 700 mW/cm^2. It should be noted that fuel utilization was not care-

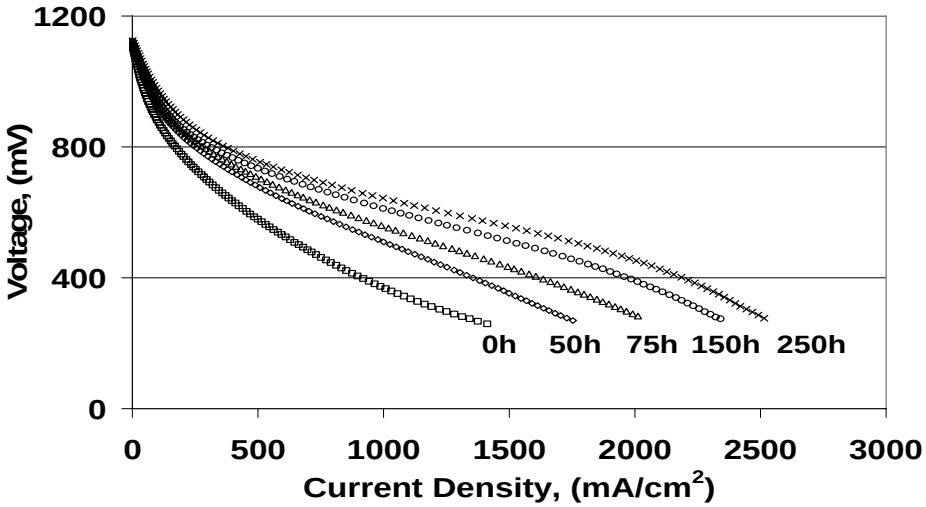

Figure 3. Voltage – Current Density Characteristics

fully monitored for this cell as it is difficult to control this metric accurately for single cell tests. However, it is known that sufficient gas flow is available such that the observed mass transfer effects are likely not associated with hydrogen or oxygen starvation, but more likely related to limitations in the back diffusion of steam on the anode or blockage by N_2 on the cathode. Tafel parameters were estimated from the polarization curves through a non-linear least squares approach described previously ([xii]). Because a reference electrode was not used in these experiments, an absolute determination of the individual anode and cathode kinetics or the exchange current density was not possible. However, relative changes in the kinetics can be useful for illustrating the improvements in the performance of the cell during the ripening process. It is assumed that these estimated Tafel slopes are associated primarily with the oxygen reduction reaction although anodic contributions cannot be neglected (xii). Tafel slopes of 69 mV/dec were initially observed which steadily decreased to about 46 mV/dec during the first 250 hours of test at a rate of 0.12 mV/dec/hour. These values are consistent with theoretical single electrode Tafel slopes which can vary from 50 mV/dec to 100 depending upon the selection of the transfer coefficient. The corresponding transfer coefficients for the estimated Tafel parameters of the cell as a function of ripening time are also presented in Table 1.

Table 1. Estimated Tafel Parameters as a function of cell run-time

Cell Time-on-stream @ 750°C	Tafel Parameter (mV/dec)	Transfer Coefficient, α
0 hours	69	0.7
50 hours	66	0.8
75 hours	55	0.9
150 hours	49	1.0
250 hours	47	1.0

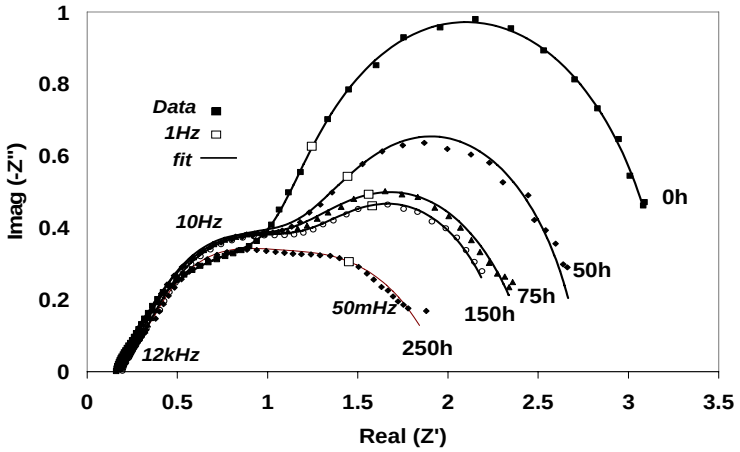

Figure 4: Impedance spectroscopy of a SOFC cell during activation as measured at different times during operation at 750°C.

EIS was used to elucidate the mechanism of the improved cell performance with increasing polarization time and the data are presented as Figure 4. As discussed previously, the galvanostatic longevity run was periodically interrupted to determine cell performance wherein EIS spectrum was taken at open circuit voltage (OCV) just after the polarization experiment. One can see that the trend of the EIS data appears to mirror the enhancement observed in the polarization curves with a steady decrease in cell resistance. Upon initial inspection, it is clear that the EIS spectra contain at least 3 time constants which are associated with the occurrence of different electrochemical processes which may include electrode mass transfer, charge transfer kinetics, and electrical conductivity. The first of these features spans approximately 0.25 Ω-cm^2 to 1 Ω-cm^2 and appears to peak at approximately 10 Hz. Closer examination of this feature appears to indicate that it contains at least two distributed elements which cannot be completely deconvoluted within the measured frequency range. It is generally thought that the first feature (>1000 Hz) is associated with anodic processes which can contribute to as much as 10% of the total observed impedance depending upon potential (12,[xiii]). The area specific ohmic resistance (ASOR), obtained from the high frequency intercept, remains relatively constant over the span of this study varying from 0.16 Ω-cm^2 measured during initial operation to 0.19 Ω-cm^2 measured at 250 hours. The ASOR is a measure of the entire cell ohmic contribution which includes contact and current collection resistances. This small increase in cell resistance is not likely associated with a change in the hermeticity

or morphology of the electrolyte but more likely due to some loss of the silver/platinum current collectors as a function of time. Only minor changes in the EIS spectra were observed over these high frequency features, however, a pronounced change in both the real and imaginary components of the resistance were observed in the low frequency region (< 2 Hz). Clearly, a significant improvement in cell capacitance was observed with the largest percentage improvement occurring within the first 50 hours of operation. This increase in capacitance is accompanied by a significant decrease in real resistance of this low frequency feature.

In an effort to quantify the performance improvement of this cell, the data in Figure 4 was modeled using equivalent electrical circuits through a non-linear least squares regression approach ([xiv]). Figure 5 presents an example of this analysis wherein a standard RC circuit was used to approximate the impedance elements of the cell during a typical EIS experiment. The notional RC features are displayed as dashed and hatched lines which illustrate the distributed impedances which occur in the fuel cell during

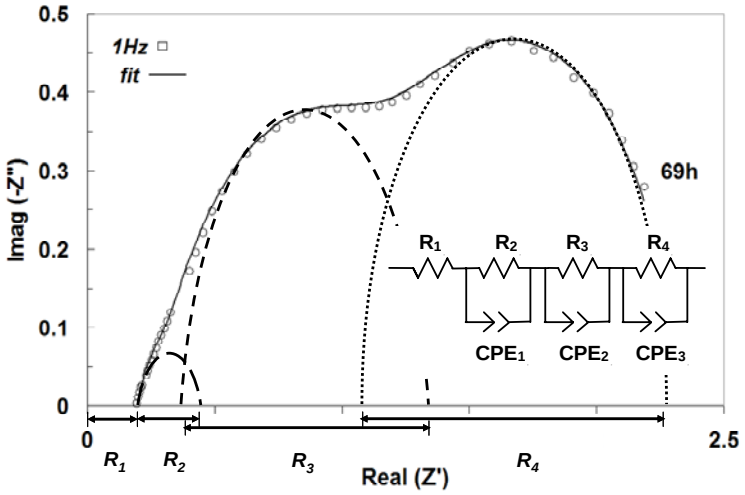

Figure 5: Example impedance spectrum with notional semicircular features illustrating the data analysis of a SOFC cell during activation (750°C).

characterization. The real resistances are obtained as the diameter of each of the semicircular features and provide a measure of the individual resistances associated with the different simultaneous processes which occur in the cell including anode and cathode kinetics, ohmic, and reactant/product transport phenomenon. Because real data cannot always be adequately modeled through a standard capacitor element, a Constant Phase Element (CPE_n) was used to account for some overlap of EIS elements in the analyzed spectra. The data in Figure 4 was regressed and the real components of the impedance are presented as Figure 6.

Inspection of Figure 6 clearly illustrates that no discernable trend in real impedance for the high frequency features is evident as a function of time-on-stream. The slopes for R_1, R_2, and R_3 are nearly zero within the margin of experimental error. As discussed previously, ASOR (R_1) averaged 0.18+/- 0.01 over the first 250 hours of operation. R_2

and R_3, which also exhibited a constant slope over the test range, averaged 0.1 +/- 0.02 and 0.9 +/- 0.01. This form of data treatment clearly highlights the significant change in the R_4 real resistance which exhibited a slope of -0.007 Ω-cm^2/hour and is responsible for nearly all of the performance improvement in the cell.

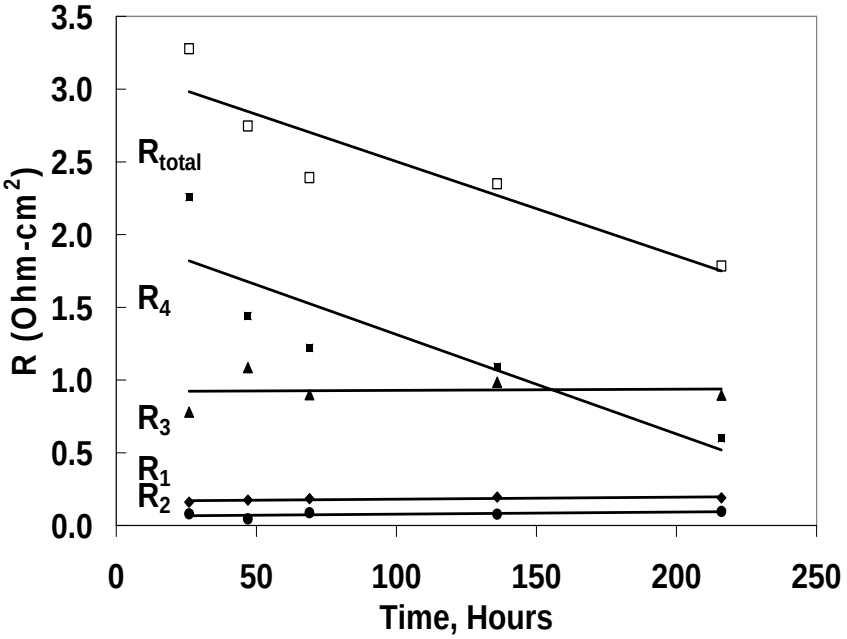

Figure 6: Real component of impedance as a function of time-on-stream (750°C).

In an effort to clarify the nature of cell activation which occurred during the galvanostatic longevity test, an experiment was performed to isolate a specific feature in EIS spectra. Two SOFC button cells were prepared with identical NiO/YSZ anodes, NiO/YSZ anode interlayers, and YSZ electrolyte. In the first cell, a mixed conducting 10 μm cathode interlayer consisting of equal parts YSZ and LSM was applied prior to application of the bulk LSM cathode while in the second cell the interlayer was omitted. After this preparation, the cell was prepared for electrochemical characterization and EIS experiments were performed. The data is presented as figure 7.

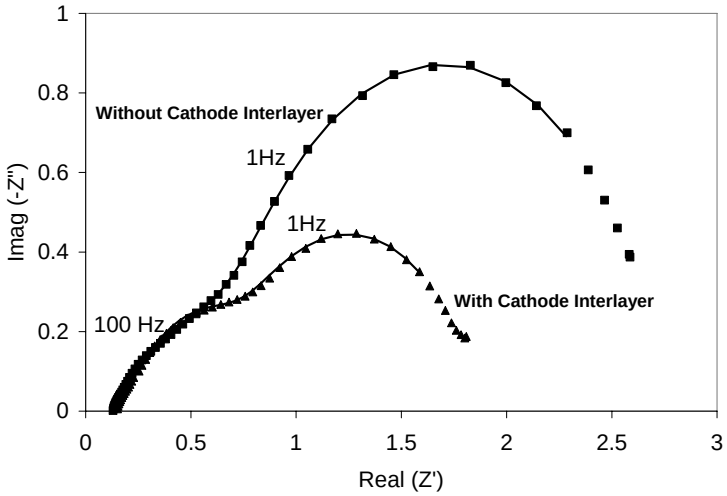

Figure 7. Impedance spectra of SOFC containing both a cathode interlayer (▲) and without cathode interlayer (■). Both specimens were measured at 800°C.

The EIS spectra in figure 6 appears similar in form and magnitude to that presented in figure 4. The high frequency features (> 25 Hz) exhibit negligible differences in the real and imaginary components of resistance (R_1, R_2, and R_3) for the specimens regardless of the presence of the cathode interlayer. As frequency is decreased, a noticeable separation of the figures becomes apparent once frequency is reduced below approximately 10Hz. The sample without the cathode interlayer, by contrast, is significantly more resistive. Both real and imaginary components of impedance were observed to increase with decreasing frequency with the real component (R_4) increasing from 1.2 Ω-cm^2 to 2.0 Ω-cm^2 for the sample with and without cathode interlayers, respectively.

What is apparent from these data is that it provides a clear indication that these low frequency (< 25 Hz) changes which were observed during the longevity test are associated primarily with the cathode/electrode interface in these cells. Furthermore, because no change in the higher frequency features of the EIS spectra were observed, it appears to indicate that these features are unrelated to cathodic processes.

Discussion

Several studies have sought to clarify the observed activation of SOFC during polarization. Jiang and coworkers have previously observed this activation phenomenon over short times (<180 min) and presented several explanations for this performance enhancement which include morphological modification of the LSM cathode and migration of SrO into the lattice to enhance cathode oxygen vacancy (ix,x). Experiments were preformed wherein several different polarization treatments (anodic and cathodic) were applied after which chemical analysis and SEM were performed. The microscopy data clearly illustrated a change in morphology from a less porous, closed LSM network to a more porous morphology with exhibiting smaller crystallites. While these studies were performed for significantly shorter times than the subject study, these results clearly support the notion that the observed long term performance enhancement is associated with a formation of an electroactive species near the cathode/electrolyte interface. Jiang presented a mechanism to explain this observation based upon an equilibrium model proposed by Mizusaki et al. which involved the reduction of the Mn_2O_3 species to MnO to promote charge compensated oxygen vacancies during operation ([xv], [xvi]). The EIS experiments presented in Figures 4 and 7 support this observation as they appear to indicate that the cell ripening process is associated primarily with the cathode cell interlayer which is mixed conducting in nature and limited to approximately 10 μm from the electrolyte. If the activation process was associated even somewhat with diffusive or electronic transport processes one would expect a much more subtle change in performance when comparing specimens with and without a cathode transition layer as seen in Figure 7. It is well accepted that the introduction of this cathode transition layer is essential for high power density performance as it promotes a mixed conducting region within the cathode and effectively extends the triple phase boundary into the bulk cathode (xii, [xvii], [xviii]). The time-induced activation of the cell appears to exhibit similar EIS changes in this low frequency region which appear to suggest that this activation is associated with an enhancement in the mixed conducting region of the cathode electrode/electrolyte interface which is know to be ~10 μm in thickness.

Conclusion

The longevity performance of a tape cast solid oxide button fuel cell with a LSM-based cathode was studied galvanostatically at several different current levels for nearly 500 hours at 750°C and at low fuel utilization. Periodically the specimen was analyzed through polarization and electrochemical impedance spectroscopy experiments. The data clearly shows a pronounced activation with time on stream. Polarization experiments showed a marked improvement of the cell from initial values of 370 mW/cm^2 at 340 mV to 910 mW/cm^2 at 470 mV measured at 250 hours. EIS experiments mirrored this improvement in performance. These experiments also indicated that the performance enhancement was primarily associated with the low frequency feature which occurred < 2 Hz. Subsequent experiments which studied the EIS response of tape cast button cells with and without a cathode transition interlayer indicated that this low frequency feature is associated with the cathodic processes. As such, there is clear evidence that the performance improvement observed during SOFC activation under polarization is related to the activation of the mixed conducting region at the interface of the cathode/electrolyte interface.

References

i. Colson-Inam, S., *Fuel Cell Today* **1,** 1 (2004).
ii. Larminie, J., A. Dicks, Fuel Cell Systems Explained, John Wiley and Sons Ltd., West Sussex, (2003).
iii. Kawada, T. and H. Yokokawa, *Key Engineering Materials*, **187**, 125 (1997).
iv. Singhal, S.C., *Solid State Ionics*, **135**, 305 (2000).
v. Charpentier, P., P. Fragnaud, D.M. Schleich, E. Gehain, *Solid State Ionics*, **135**, 373 (2000)
vi. Kim, J.W., A.V. Virkar, K.Z.Fung, K. Mehta, S.C. Singhal, *J. Electrochem. Soc*., **146**, 69 (1999)
vii. Brant, M.C., T. Matencio, L. Dessemond, R.Z. Domingues, *Solid State Ionics*, **177**, 915 (2006).
viii. Jiang, S.P., J.G. Love, J.P. Zhang, M. Hoang, Y. Ramprakash, A.E. Hughes, S.P.S. Badwal, *Solid State Ionics*, **121**, 1 (1999).
ix. Wang, W. and S.P. Jiang, *J. Solid State Electrochem*, **8**, 914-922 (2004).
x. Jiang, S.P., *J. Solid State Electrochem*, **11**, 93-102 (2007).
xi. Xiao, H. and T.L. Reitz, In Solid-State Ionic Devices I.V., in: E.D. Wachsman, F.H. Garzon, E. Traversa, R. Mukundan, V. Birss (Eds.), The Electrochemical Society Proceedings Series, NJ, (2005).
xii. Reitz, T.L. and H. Xiao, *J. Pwr Sources*, **161**, 1, 437-443 (2006).
xiii. Wagner, N., W. Schnurnberger, B. Muller, M. Lang, *Electrochim. Acta* **43** 24, (1998) 3785–3793.
xiv. Macdonald, J.R., Impedance Spectroscopy, John Wiley and Sons, New York, NY, 1987.
xv. Mizusaki, J, N. Mori, H. Takai, Y. Yonemura, H. Minamiue, H. Tagawa, M. Dokiya, H. Inaba, K. Naraya, T. Sasamoto, T. Hashimoto T, *Solid State Ionics*, **161**, 209 (2000)
xvi. Lee, H.Y., W.S. Cho, S.M. Oh, H-D Wiemhofer, W. Gopel, *J. Electrochem Soc*, **142**, 2659, (1995)
xvii. Zhao, F., A. Virkar, *J. Power Sources* **141** 79–95, (2005)
xviii. Kim, J.D., G.D. Kim, J.W. Moon, Y.I. Park, W.H. Lee, K. Kobayashi, M. Nagai, C.E. Kim, *Solid State Ionics* **143** 379–389, (2001)